IOPscience iopscience.iop.org

Home Search Collections Journals About Contact us My IOPscience

Raman scattering and non-linear optical properties in $Li_2B_4O_7$

This article has been downloaded from IOPscience. Please scroll down to see the full text article.

2005 J. Phys.: Condens. Matter 17 7441

(http://iopscience.iop.org/0953-8984/17/46/027)

View the table of contents for this issue, or go to the journal homepage for more

Download details:
IP Address: 129.252.86.83
The article was downloaded on 28/05/2010 at 06:48

Please note that terms and conditions apply.

INSTITUTE OF PHYSICS PUBLISHING JOURNAL OF PHYSICS: CONDENSED MATTER

J. Phys.: Condens. Matter **17** (2005) 7441–7454 doi:10.1088/0953-8984/17/46/027

Raman scattering and non-linear optical properties in $Li_2B_4O_7$

A Elbelrhiti Elalaoui, A Maillard[1] and M D Fontana

Laboratoire Matériaux Optiques, Photonique et Systèmes, UMR CNRS 7132, Université de Metz and Supélec, 2 rue E Belin 57070 Metz, France

E-mail: maillard@metz.supelec.fr

Received 16 June 2005, in final form 26 September 2005
Published 2 November 2005
Online at stacks.iop.org/JPhysCM/17/7441

Abstract

A complete Raman scattering study on a lithium tetraborate single crystal is reported. The frequency and scattered intensity of Raman modes are carefully determined in the various geometrical configurations. These Raman data are then used to relate to the electro-optical and non-linear optical properties. Raman scattering efficiencies of $A_1(a)$, $A_1(b)$ and E phonons are consistent with the values of the EO coefficients r_{13}, r_{33} and r_{51} respectively.

1. Introduction

Borate crystals, such as $Li_2B_4O_7$ (LTB), LiB_3O_5 (LBO), $CsLiB_6O_{10}$ (CLBO) and β-BaB_2O_4 (BBO), have received much attention because of their excellent properties for nonlinear optics.

One of them, lithium tetraborate, $Li_2B_4O_7$ (LTB), is rather known as a piezoelectric crystal and attracted attention as a suitable substrate for surface acoustic wave (SAW) devices because of its high electrical–mechanical coupling coefficient [1]. It may be used as a dielectric resonator at about 10 MHz [2] and low-loss SAW filter at 213 MHz [3]. Recently, an LTB crystal was proved to be interesting for the conversion of frequencies including the second (532 nm), fourth (266 nm) and fifth (213 nm) harmonic generation of the Nd:YAG laser [4].

The crystal structure of LTB has been determined by Krogh-Moe [5]. Its structure at room temperature is tetragonal with space group C_{4v}^{12} and point group $4mm$ with the polar axis along the crystallographic c-axis [6]. The unit cell dimensions are $a = 9.477$ Å and $c = 10.286$ Å [7]. The structure with eight formula units of LTB contains a basic building block of two BO_4 tetrahedra linked by a common oxygen atom, forming a B_2O_7 group joining two planar triangles BO_3 using the common oxygen atoms (figure 1).

In this paper, we aim to relate the Raman scattering efficiencies to the electro-optical (EO) and nonlinear optical (NLO) effects of LTB and thus to estimate the various contributions to EO coefficients. We present a complete study of the Raman spectra, in order to determine

[1] Author to whom any correspondence should be addressed.

 © 2005 IOP Publishing Ltd Printed in the UK

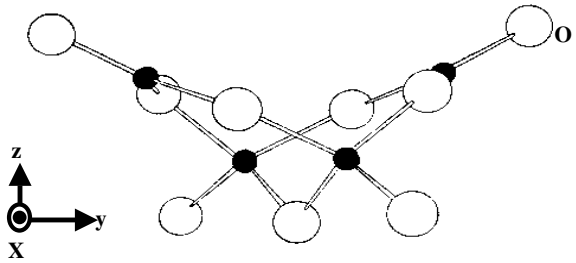

Figure 1. The basic structural unit of the LTB. (Black disc = boron; white disc = oxygen.)

the characteristics of all modes of vibration which are then assigned to structural groups. For this, we used several single crystals, grown from the melt by the Czochralski technique [8]. Some Raman results are then used to estimate the ionic and electronic contributions of the EO coefficients. In this way, the origin of the EO and NLO properties of LTB is interpreted.

2. Raman data

2.1. Raman scattering measurements

The irreducible representation for the normal vibration modes, provided by the group theory, is given by [9] $\Gamma = 19A_1 + 19A_2 + 19B_1 + 19B_2 + 40E$. Among these, the A_2 modes are Raman inactive whereas only the A_1 and E modes associated with a dipolar phonon moment, are both Raman and infrared active. Whereas one A_1 and one E are acoustic modes, the Raman active optical modes are $\Gamma = 18A_1 + 19B_1 + 19B_2 + 39E$.

The Raman polarizability tensors are written in the crystallographic tetragonal axis system (X, Y, Z) as

$$A_1(Z) = \begin{bmatrix} a & \cdot & \cdot \\ \cdot & a & \cdot \\ \cdot & \cdot & b \end{bmatrix} \qquad B_1 = \begin{bmatrix} c & \cdot & \cdot \\ \cdot & -c & \cdot \\ \cdot & \cdot & \cdot \end{bmatrix} \qquad B_2 = \begin{bmatrix} \cdot & d & \cdot \\ d & \cdot & \cdot \\ \cdot & \cdot & \cdot \end{bmatrix}$$

$$E(X) = \begin{bmatrix} \cdot & \cdot & e \\ \cdot & \cdot & \cdot \\ e & \cdot & \cdot \end{bmatrix} \qquad E(Y) = \begin{bmatrix} \cdot & \cdot & \cdot \\ \cdot & \cdot & e \\ \cdot & e & \cdot \end{bmatrix}.$$

The letter in brackets denotes the direction of the mode polarization for the polar (infrared active) phonon. Table 1 compiles the scattering geometries which can be used to detect the various optical modes. The direct and separate detection of the B_1 spectrum is impossible in the scattering geometries according to the (X, Y, Z) system. Therefore, in the earlier Raman studies [9, 10] the frequencies of the B_1 phonons were indirectly deduced from the comparison of two spectra: X(YY)Z which provides $A_1 + B_1$ phonons and X(ZZ)Y which yields A_1 lines. In order to avoid any ambiguity in the assignment of the B_1 modes, we have carried out the direct measurement of the B_1 spectrum which can be achieved in the (X′, Y′, Z) axis system, when the X′ and Y′ axes are turned through 45° with respect to the X and Y axes.

Several LTB samples were thus cut according to the two coordinate axis systems used in our Raman measurements in order to get the complete investigation of all optical phonons. Raman spectra were recorded with a Spex double monochromator at room temperature, using the 514.5 nm line of a Ar ion laser as the exciting line.

It has to be mentioned that all spectra are normalized in intensity even if they were recorded in different scattering planes. This was achieved in considering the same phonons recorded in two different scattering planes (see table 1), allowing the phonon relative intensity comparison.

Table 1. Raman scattering configurations used to detect the optical phonons for the various symmetries. Intermediate polarization between the LO and TO components is denoted IO.

Scattering plane	Configurations	Modes
XY	X(ZZ)Y	A_{1TO}(b)
	X(ZX)Y	$E_{TO} + E_{LO}$
	X(YX)Y	B_2(d)
XZ	X(ZX)Z	E_{IO}
	X(ZY)Z	E_{TO}
	X(YY)Z	A_{1IO}(a) + B_1(c)
	X(YX)Z	B_2(d)
$X\overline{X}$	X(ZY)$\overline{X}$	E_{TO}
	X(ZZ)$\overline{X}$	A_{1TO}(b)
	X(YY)$\overline{X}$	A_{1TO}(a) + B_1(−c)
$Z\overline{Z}$	Z(XX)$\overline{Z}$	A_{1LO}(a) + B_1(+c)
	Z(YY)$\overline{Z}$	A_{1LO}(a) + B_1(−c)
	Z(XY)$\overline{Z}$	B_2(d)
X′Y′	X′(Y′X′)Y′	B_1(−c)
	X′(ZZ)Y′	A_{1TO}(b)

This normalization was needed for a correct line assignment to vibrational modes, as well as for the evaluation of the electro-optic and SHG coefficients.

2.2. Raman spectra

2.2.1. A_1 and B_1 modes. The A_{1TO} phonons can be directly provided by the X(ZZ)Y spectrum only. They are attributed to well resolved lines shown in figure 2(a) and detected at 156, 255, 296, 340, 491, 507, 722, 779, 976, 1030, 1162 and 1176 cm^{-1}.

Ambiguities on the origin of wide bands lying around 200 and 1400 cm^{-1} in our X(ZZ)Y spectrum remain so that only 12 lines could be clearly assigned to A_{1TO} phonons instead of the 18 expected modes. Our results thus do not differ strongly from the earlier data [9, 10] and do not yield a complete view of the A_1 phonons. Therefore, we additionally investigated the back-scattering spectrum X(YY)$\overline{X}$, in figure 2(b), which gives rise to A_{1TO} and B_1 phonons. This spectrum is compared in figure 2(c) with the purely B_1 spectrum carried out in the X′(Y′X′)Y′ geometry. B_1 modes are unambiguously obtained from this spectrum in contrast with previous studies, so that the lines attributed to A_{1TO} can be clearly extracted from the comparison with the X(YY)$\overline{X}$ spectrum. The spectrum X(YY)$\overline{X}$ differs from the spectrum X(ZZ)Y in the relative intensities of the lines since it involves component 'a' of the Raman tensor instead of 'b'. Moreover, the spectrum X(YY)$\overline{X}$ yields some features which were undetected or hidden in the other spectrum so that the assignment of all expected A_{1TO} lines was achieved.

A_{1LO} phonons were detected together with B_1 modes in the Z(YY)$\overline{Z}$ spectrum as shown in figure 1(d). They are generally lying in a very close vicinity of the positions of A_{1TO} phonons. Revealing the weak polar character of most A_1 modes, solely five A_1 modes display a significant TO–LO splitting which allows us to calculate the oscillator strength, as

$$\Delta\varepsilon_k^m = \varepsilon_k(\infty)\left(\frac{\omega_{LO,m}^2}{\omega_{TO,m}^2} - 1\right)\prod_{j\neq m}\left[\frac{\omega_{LO,j}^2 - \omega_{TO,m}^2}{\omega_{TO,j}^2 - \omega_{TO,m}^2}\right]. \quad (1)$$

The frequencies of all A_{1TO} and A_{1LO} phonons are reported in table 2, as well as the oscillator strengths together with the respective integrated intensities of the corresponding

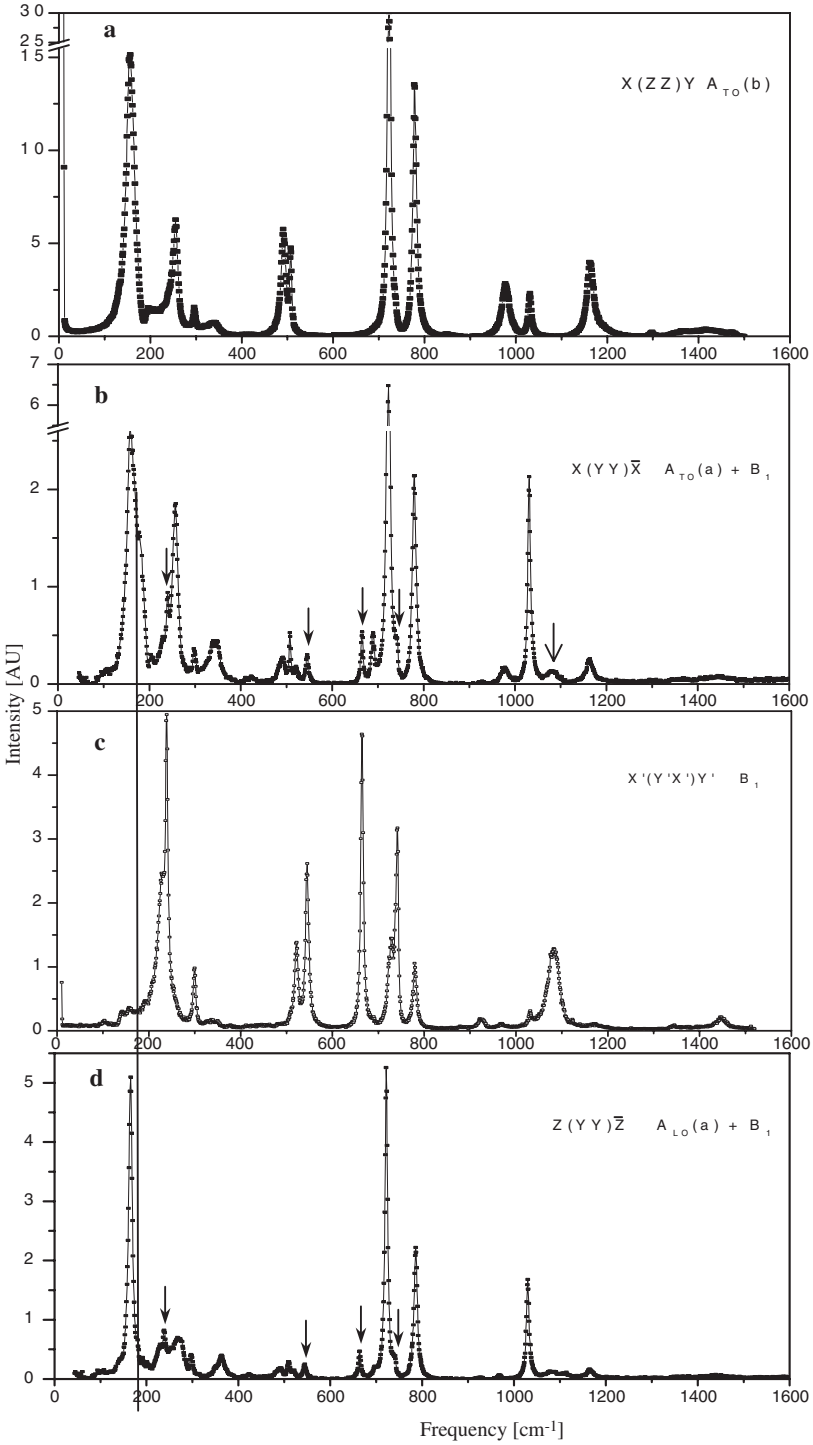

Figure 2. Raman spectra of the A_1 and B_1 modes. The arrows indicate the positions of B_1 lines.

Table 2. Characteristics (frequency and integrated intensity (AU, arbitrary units)) of the A_1 modes. The oscillator strength of the polar modes (bold) is given between brackets. The vibration frequencies are compared with those of the literature.

A_{1TO}				A_{1LO}(a)	
Frequency (cm^{-1})					
Our results	Furusawa [10]	Paul [9]	Integrated intensity of A_{1TO}(a) (AU)	Frequency (cm^{-1})	Integrated intensity (AU)
156 (0.44)	156	153	287	**165**	44
165			295	165	46
180	194	196	135	180	14
255			133	256	18
255 (0.48)	255	262	143	**274**	20
296	295	299	22	298	3
341 (0.26)	340	351	150	**362**	13
489	490	425	58	489	6
506 (0.03)	506	495	21	**509**	3
520		508	13	520	1
687 (0.07)	706		35	**697**	2
722	720	724	540	722	74
740		781	9	740	2
778 (0.04)	777	849	205	**785**	35
976	976	980	29		
1030	1028	1034	162	1030	21
1161 (0.02)	1161	1166	36	**1166**	5
1176			15		
Band 1327–1497		Band 1350–1550			

lines. 18 A_{1TO} and 16 A_{1LO} phonons were thus attributed so that only two A_{1LO} phonons are missing.

The low-frequency spectrum was paid special attention. Data recorded at low frequency in $X(YY)\overline{X}$ and $Z(YY)\overline{Z}$ configurations are shown and compared in figure 3. Spectra are fitted to a sum of damped oscillators, to extract the frequency and damping of each mode. Three A_{1TO} and two A_{1LO} phonons are derived from these spectra and fitting procedure. Lines at 165 and 180 cm^{-1} are found in both A_{1TO} and A_{1LO} spectra, reflecting the existence of two non-polar A_1 modes at these frequencies. In a first view, the A_{1LO} spectrum does not exhibit any evidence of the LO line associated with the A_{1TO} phonon occurring at 156 cm^{-1}. As the TO line is relatively intense, the LO component should be detected in the spectrum $Z(YY)\overline{Z}$. In fact we noted that the intensity of the LO peak at 165 cm^{-1} is larger than that of the TO line to which it should correspond, whereas the opposite situation is expected. Indeed, as shown in table 2 for each polar or non-polar A_1 mode, the intensity of the LO line is much smaller than that of the TO component. The fact that this feature fails for the LO peak at 165 cm^{-1} proves that the peak around 165 cm^{-1} is due to two phonons lying at the same frequency, one attributed to the LO component of a polar A_1 mode and associated with a component at 156 cm^{-1}, the other arising from a non-polar mode. It should be mentioned that the same explanation holds for the peak at 255 cm^{-1}.

2.2.2. B2 modes. According to table 1, B_2 phonons can be determined from several configurations and various scattering planes. In principle all spectra can provide the B_2 lines at the same positions. However, as shown in figure 4, spectra X(YX)Y and X(YX)Z show

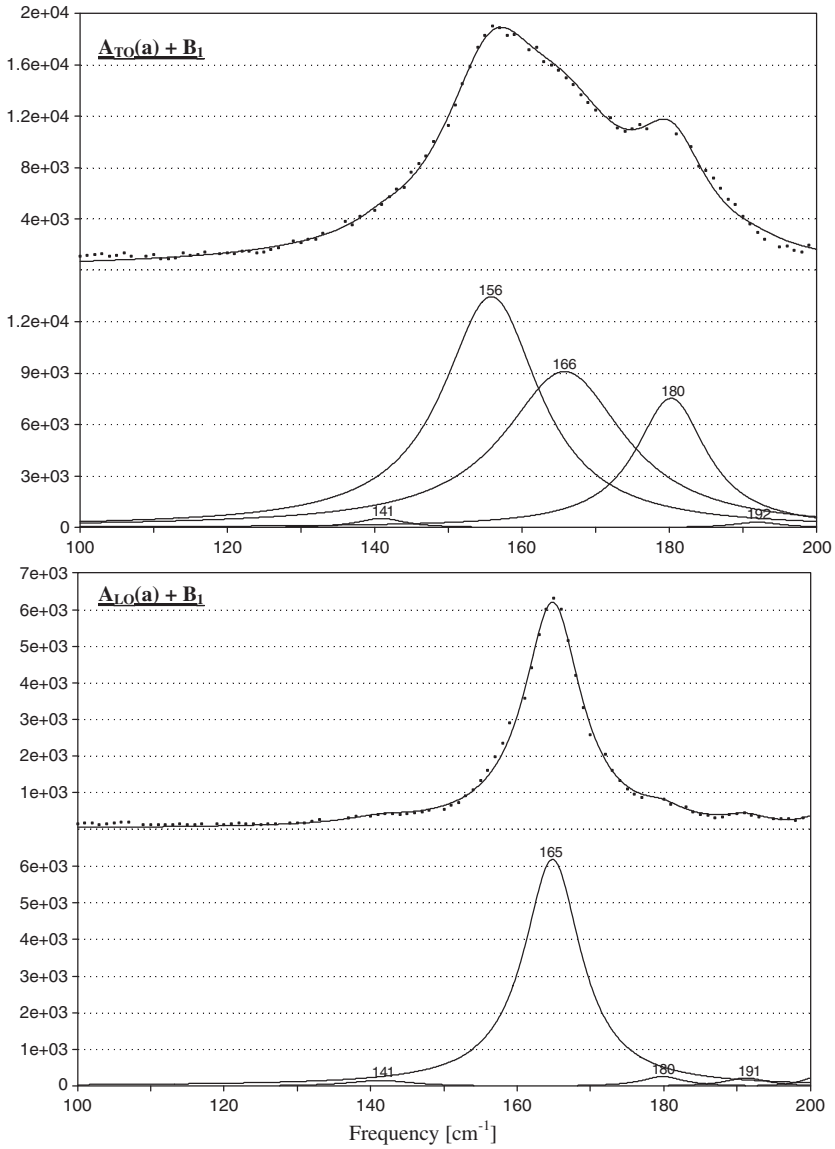

Figure 3. Low-frequency X(YY)$\overline{X}$ and Z(YY)$\overline{Z}$ spectra. Spectra fit to a sum of damped oscillators. Continuous lines represent the calculated spectra. The 141 cm^{-1} peak is a leakage of a strong E_{TO} mode.

significant differences in the line shape. In fact this arises from the leakage of A_1 and B_1 lines in the X(YX)Z spectrum. This is due to the fact that A_1 and B_1 phonons, detected in the X(YY)Z spectrum in the same scattering plane XZ, are very intense (more than five times larger than B_2 phonons), so that a slight disorientation of the analyser with respect to the crystal axes is sufficient to allow the observation of A_1 phonons in the B_2 spectrum. In our opinion this leakage by modes of different symmetries caused an erroneous assignment of B_2 modes in earlier studies [9, 10]. B_2 modes were detected in the X(YX)Y configuration with a better confidence than in the X(YX)Z and Z(YX)$\overline{Z}$ geometries. Therefore, our results reported in

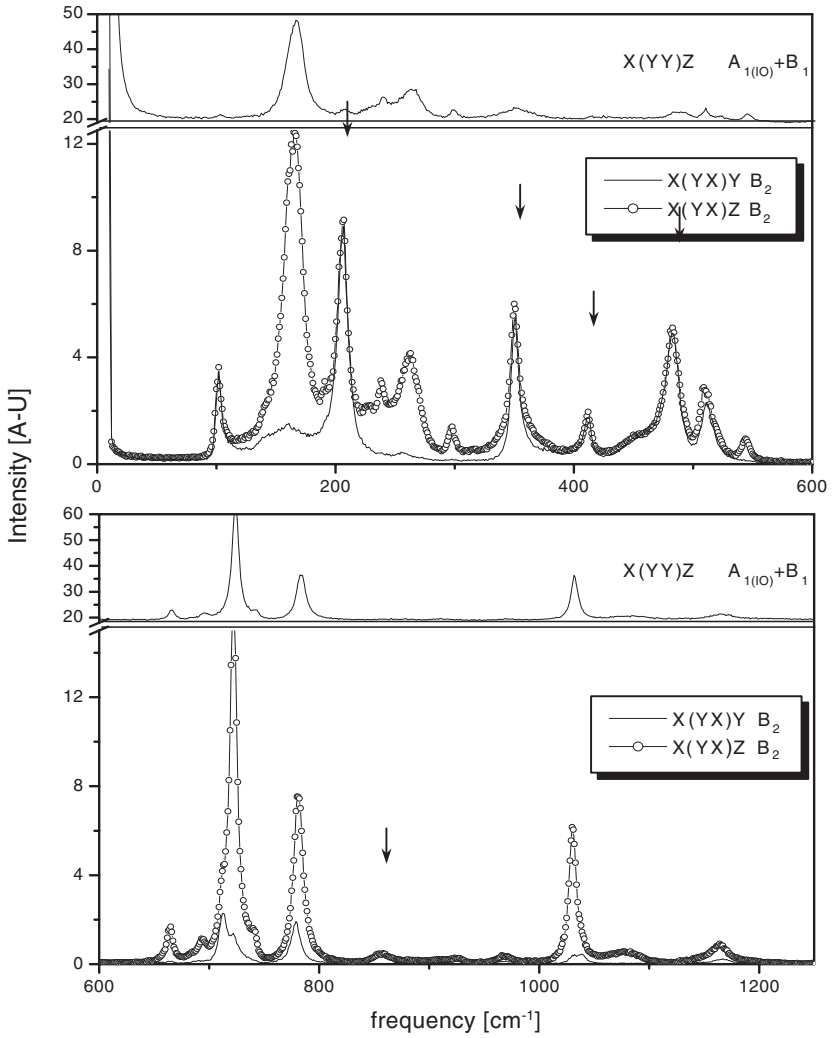

Figure 4. The B_2 spectra recorded in several configurations. We represent for comparison the $A_{1(IO)} + B_1$ modes responsible for the strong leakage of the B_2 spectrum in the X(YX)Z scattering plane. The arrows indicate some B_2 lines as derived from the comparison.

table 3 show some disagreements compared with the literature. This corroborates that the measurement of the X(YX)Y spectrum considered in our study allows us to achieve a better assignment of the B_2 modes.

2.2.3. E modes. E_{TO} phonons are detected from the spectrum X(ZY)Z whereas the $E_{TO} + E_{LO}$ lines are observed in the spectrum X(ZX)Y. As shown in figure 5 both spectra are very similar to each other. Some slight differences are displayed in the low-frequency range between 100 and 250 cm^{-1}, which is reported in figure 6. A careful comparison between spectra allows us to extract the E_{LO} phonons which occur at frequencies different from those of the TO phonons.

As a consequence only three E modes possess a significant oscillator strength which can be calculated according to equation (1): the phonons lying at 103 cm^{-1} (LO at 111 cm^{-1})

Table 3. Frequencies (in cm^{-1}) of the B_1 and B_2 phonons compared with the previous data reported in the literature.

B_1: X′(Y′X′)Y′			B_2: X(YX)Y		
Our results: X′(Y′X′)Y′	Furusawa [10]	Paul and Taylor [9]	Our results	Furusawa [10]	Paul and Taylor [9]
100	102	100	102	102	100
		132	110	144	
191	194	194		164	162
	205		184	188	
227			206	205	213
239	238	236	350	351	351
	264	241	361		358
299		319	392		
	348	372	411	412	413
521		523	460		447
545		547	482	482	488
665	544	668	512	510	515
	644	685	689		
	691	695	713	711	715
729			730	730	
739	740		779	778	782
742		743	857	856	858
	762			932	
	794		1039	1036	1042
		886	1167		1171
924		914			1309
1052					
1074		1070			
1084					
1091		1089			
1124					
1447					

117 cm^{-1} (LO at 123 cm^{-1}) and 201 cm^{-1} (LO at 209 cm^{-1}). All TO and LO phonons are compiled in table 4.

25 lines $E_{TO}+E_{LO}$ have been detected by Paul and Taylor [9]. In our study the comparison between the spectra E_{TO} and $E_{TO}+E_{LO}$ allowed us to detect 13 additional E lines compared to Paul and Taylor's work and to evaluate the LO–TO splitting. Thus our spectrum (figure 6) exhibits the existence of the LO and TO components of a polar mode lying at 201 and 209 cm^{-1} respectively while Paul and Taylor assigned only one non-polar mode at 208 cm^{-1}. In the low-frequency range four additional modes were detected at 117, 139, 161 and 193 cm^{-1} in our study.

2.3. Mode assignment

The assignment of the internal vibrational modes in LTB is rendered difficult by the structure complexity. Even if the rigid structure is made up of BO_4 tetrahedra and the planar BO_3 triangles, these groups are not independent of each other in the crystal. The crystallographic analysis of the structure shows the existence of four grouping forms: BO_3, BO_4, LiO_4 and LiO_6 [11]. We establish our assignment on the knowledge of the frequencies of normal modes for the free groups BO_4 and BO_3 [9, 12], and on some similarities with other borate compounds ($CsLiB_6O_{10}$, LiB_3O_5 ...). Results are presented in table 4.

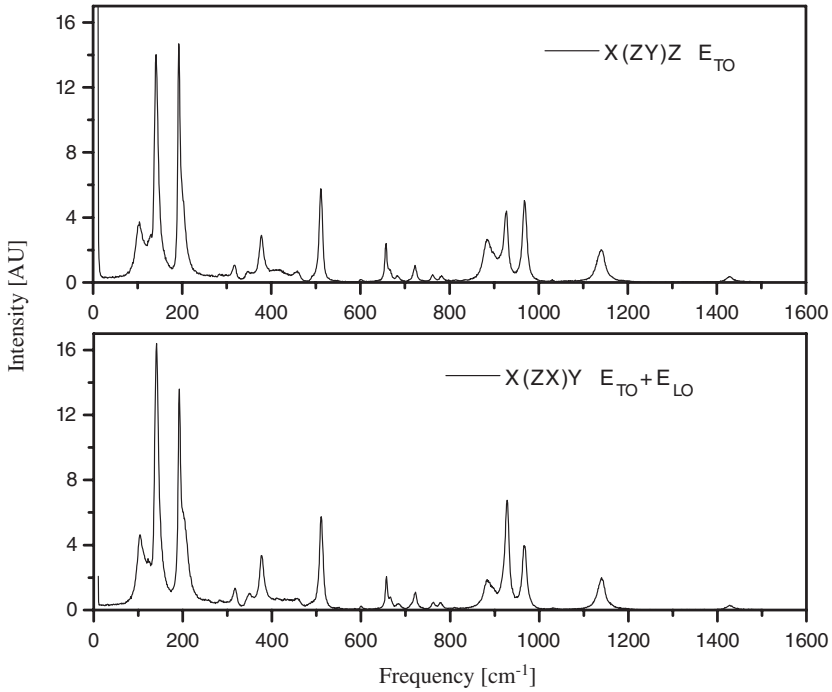

Figure 5. E mode Raman spectra.

3. Origin of EO and NLO properties in LTB

Above acoustic resonances, the EO Pockels effect results from two mechanisms. The first process comes from the direct modulation of electrons by the external electric field whereas the lattice remains rigid, and the second process arises from the indirect modulation via the electron–phonon interaction. Both these processes give rise to the electronic and the ionic contribution r^{E} and r^{I} respectively. The contribution of each phonon mode to the EO coefficient can be thus expressed as

$$\delta r_{ijk} = \left.\frac{\partial \chi_{ij}^{-1}}{\partial E_k}\right|_{Q_k} + \left.\frac{\partial \chi_{ij}^{-1}}{\partial Q_k}\right|_{Ek} \frac{\partial Q_k}{\partial E_k}$$

where Q_k is the normal coordinate along the k direction associated with the ionic motion in a particular phonon mode, χ_{ij} is the (ij) component of the linear susceptibility at the optical (laser) frequency and E the modulating electric field.

Both electronic and ionic parts of the EO coefficient can be evaluated from Raman scattering data via the relationship between electro-optic, Raman polarizability and oscillator parameters [13–17].

Thus we have for the mth polar phonon

$$\delta r_{ij,k}^{\mathrm{I}(m)} = -\frac{\varepsilon_0}{n_i^2 n_j^2} \frac{\sqrt{\Delta\varepsilon_k^{(m)}}}{\omega_{\mathrm{TO}}^{(m)}} \alpha_{ij,k}^{(m)} \tag{2}$$

$$\delta r_{ij,k}^{\mathrm{E}(m)} = -\frac{\varepsilon_0}{n_i^2 n_j^2} \frac{\sqrt{\Delta\varepsilon_k^{(m)}}}{\omega_{\mathrm{TO}}^{(m)}} [n_k^2 \beta_{ij,k}^{(m)} - \alpha_{ij,k}^{(m)}] \tag{3}$$

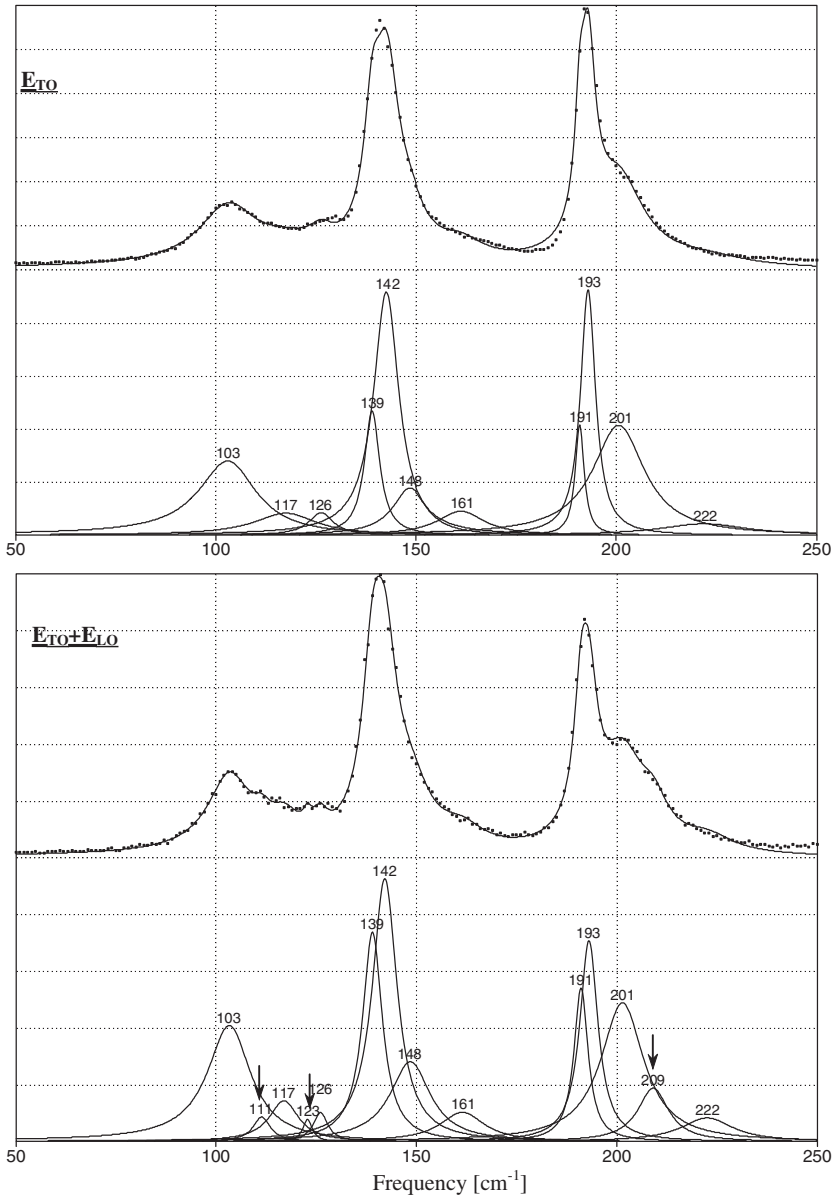

Figure 6. Comparison of the low-frequency X(ZX)Y spectra. Spectra are fitted to a sum of damped oscillators. The arrows indicate the position of E_{LO} phonons deduced from the comparison.

where n is the refractive index, ε_0 the dielectric permittivity of the vacuum, $\Delta\varepsilon^{(m)}$ the oscillator strength of the mth mode and α and β are Raman differential polarizabilities defined as derivatives of the electronic susceptibility:

$$\alpha_{ij,k} = \frac{\delta\chi_{ij}}{\delta Q_k^{\mathrm{TO}}}; \qquad \beta_{ij,k} = \frac{\delta\chi_{ij}}{\delta Q_k^{\mathrm{LO}}}.$$

Table 4. Frequency (in cm^{-1}) and assignments of the LTB vibrational modes. The oscillator strength of the polar modes (bold) is given between brackets.

B_2	B_1	A_1	E	Assignments
102; 110; 184	100	**157_165**; 165; 180	**103_111** (0.69); **117_123** (0.14); 126; 139; 142; 148; 161	External modes
206	191		191; 193; **201_209** (0.21)	BO_4 bond bending [9]
	227; 339; 299	255; 274; 296	222; 253; 290	LiO_6 vibration [19]
			316	
350; 361 392; 411; 460; 482		**341_362** 489	349; 377 412; 457; 483	BO_4 symmetric stretch [9, 21] LiO_4 vibration [19, 22]
512		**506_509**	511	BO_4 symmetric stretch [23]
	521; 545	520		BO_3 deformation [12]
689; 713	665	**687_698**; 722	600; 657; 666; 684; 722	BO_3 asymmetric deformation [9, 21]
730	729; 739; 742	740	762	BO_3 symmetric deformation [21]
779; 857	924	776; **778_785**	780; 813; 884; 899; 917; 928	BO_4 asymmetric stretch [20, 22]
	1052	976	968	BO_3 symmetric stretch [9, 21]
1039; 1167	1074; 1084; 1091; 1124	1030; **1161_1166**; 1176	1031; 1132; 1142; 1166	BO_4 distortion [7, 21]
	1447	Band 1412	1428	BO_3 symmetric stretch [21]

The Raman polarizabilities can be calculated from the Raman-scattering cross section for the TO and LO lines respectively as [13, 14]

$$S_{ij,k}^{\mathrm{TO},m} \propto \frac{g_{ij,k}^{\mathrm{TO}}[n(\omega_{\mathrm{TO},m})+1]\omega_{\mathrm{L}}^4}{\omega_{\mathrm{TO},m}^2}\alpha_{ij,k}^{(m)^2} \tag{4}$$

$$S_{ij,k}^{\mathrm{LO},m} \propto \frac{g_{ij,k}^{\mathrm{LO}}[n(\omega_{\mathrm{LO},m})+1]\omega_{\mathrm{L}}^4}{\omega_{\mathrm{LO},m}^2}\beta_{ij,k}^{(m)^2} \tag{5}$$

where $\omega_{\mathrm{TO},m}$ and $\omega_{\mathrm{LO},m}$ are the frequencies of TO and LO components for the mth phonon, $n(\omega)$ is the Bose–Einstein factor and g is the factor dependent only on the scattering geometry. ω_{L} is the input laser frequency (much larger than phonon frequencies).

The ionic and electronic parts of the EO coefficient can thus be obtained by summation of all contributions described by equations (4) and (5). Obviously, only the polar modes, i.e. those with a non-zero oscillator strength, are accounted for.

In fact, the absolute calculations of the EO coefficients require the knowledge of the proportional factor introduced in equations (4) and (5). This factor depends on the experimental conditions related to the spectrometer (resolution), the crystal (absorption) and the laser (input power).

The determination of the absolute values of the EO coefficient is therefore not so easy that it could be more appropriate to calculate relative quantities such as the ratio $r_{ij,k}{}^{\mathrm{I}}/r_{ij,k}{}^{\mathrm{E}}$ between

Table 5. Symmetry correspondence between Raman modes and EO coefficients.

Configurations			
TO	LO or TO + LO	Raman mode	EO coefficient
X(YY)X ⇒ $A_{1TO}(a) + B_1(-c)$	Z(YY)Z ⇒ $A_{1LO}(a) + B_1(-c)$	$A_1(a)z$	r_{13}
X(ZZ)Y ⇒ $A_{1TO}(b)$ X(ZZ)X ⇒ $A_{1TO}(b)$ Y(ZZ)Y ⇒ $A_{1TO}(b)$		$A_1(b)z$	r_{33}
X(ZY)Z ⇒ $E_{TO}(e)y$	X(ZX)Y ⇒ $E_{TO}(e)x + E_{LO}(e)x$	E(e)	r_{51}

the ionic and electronic EO contributions or ${r_{ij,k}}^{\mathrm{I}}/{r_{lm,n}}^{\mathrm{I}}$ between the ionic contributions of two different EO coefficients.

Indeed, if the experimental conditions such as the input laser power and the spectrometer resolution remain constant during all measurements the Raman intensities can be compared between two different configurations.

We applied the above procedure to LTB and we estimated the electro-optic coefficients by means of our Raman data recorded in the various geometries.

Values are then compared with the direct EO measurements and experimental SHG data [18]. The electronic contribution ${r_{ijk}}^{\mathrm{E}}$ was in fact derived from SHG coefficients $d_{k,ij}$ as

$$r^{E}_{ij,k} = -\frac{4}{n_i^2 n_j^2} d_{k,ij}.$$

Indeed, it is recalled that the EO Pockels effect is a second order non-linear optical process in which one field, the modulating electric field, has a varying frequency that is generally smaller than the frequency of the second field, the laser field.

As the modulating frequency reaches the optical frequency, the EO process is equivalent to the second harmonic generation.

Before calculations it is necessary to establish in table 5 the symmetry correspondence of the Raman configurations with EO coefficients, as well as the experimental configurations used to determine the characteristics of modes TO and LO of the LTB. We can note that only the polar Raman modes A_1 and E play a role in the mechanisms at the origin of EO and NLO properties. In other terms, this means that no electric field or dipolar moment is associated with B_1 and B_2 phonons which should be able to modulate the susceptibility. The study of the B_1 and B_2 spectra was nevertheless useful for the normalization of the peak intensity during the method to go from one configuration to another. We can also notice that the EO coefficients r_{13} and r_{33}, although they are coupled with the same phonons A_1, are characterized by two different differential polarizabilities 'a' and 'b' respectively. Finally, we can note that the electronic contribution of the coefficient r_{33} is not reachable, because the $A_{1LO}(b)$ phonons cannot be measured.

At last, the EO (relative) coefficients are estimated from Raman scattering data and compared with the direct experimental values in table 6. For this, we calculated the Raman scattering cross section for the TO and LO lines recorded in the various configurations. It is recalled that intensities are normalized to account for the change of scattering plane. In addition to scattered intensities we use in the calculations (see equations (4) and (5)) the oscillator strength as determined via equation (1).

We report in table 6 the relative quantities as derived from Raman data, which are compared with the values directly deduced from direct EO [19] and SHG [18] measurements.

Table 6. Relative ionic and electronic electro-optic coefficients as calculated from Raman data. These values are compared with direct EO [19] and SHG [18] measurements.

	From Raman data	From direct measurements [18, 19]
$\frac{r^I_{13}}{r^I_{33}}$	0.98	1.
$\frac{r^I_{13}}{r^I_{51}}$	2.2	23
$\frac{r^I_{13}}{r^E_{13}}$	13	93
$\frac{r^I_{51}}{r^E_{51}}$	6.1	3.2
$\frac{r^E_{13}}{r^E_{51}}$	1	0.8

A fairly good agreement is obtained in the relative coefficients $r^{\mathrm{E}}_{13}/r^{\mathrm{E}}_{51}$, $r^{\mathrm{I}}_{51}/r^{\mathrm{E}}_{51}$, $r^{\mathrm{I}}_{13}/r^{\mathrm{I}}_{51}$ and $r^{\mathrm{I}}_{13}/r^{\mathrm{I}}_{33}$.

Calculations show that large contributions of the EO coefficients come from the two lowest-frequency phonons which exhibit both strong oscillator strength and large scattered intensities.

A relative discrepancy between indirect (Raman) and direct values is noted in $r^{\mathrm{I}}_{13}/r^{\mathrm{I}}_{51}$ and $r^{\mathrm{I}}_{13}/r^{\mathrm{E}}_{13}$. However, the fact that the Raman scattering cross section of the E_{TO} phonons is one order of magnitude lower than the intensity of A_{1TO} is consistent with the fact that the EO coefficient r^{I}_{51} is much smaller than the coefficients r^{I}_{13} and r^{I}_{33}.

Therefore it could be pointed out that the hierarchy between the various EO coefficients was found via calculations derived from Raman data.

This shows that the above described method can provide the relative order of magnitude in EO and SHG coefficients from Raman data, without requiring long-time measurements and special crystal sizes, as in the direct measurements. The relative change due to a doping or an ion substitution could be estimated as well.

4. Conclusions

We have measured the Raman spectrum of the lithium tetraborate single crystal at room temperature in a wide frequency range up to 1600 cm^{-1}. We have detected, for the first time, the B_1 and A(a) modes, and we have obtained nearly all phonon modes (18 A_1, 18 B_1, 18 B_2 and 38 E) predicted by the group theory.

The attribution of the vibrational modes of LTB, recorded in the various spectra, was carried out according to structure built from four groups BO_3, BO_4, LiO_4 and LiO_6. The spectra present two distinct ranges:

(1) 0 at 190 cm^{-1} corresponds to the external vibrations due to network rotations and translations
(2) 190 at 1600 cm^{-1} corresponds to the internal vibrations due to the motions of the four groups.

We have estimated the ionic and electronic contributions to EO coefficients from the measurement of scattered Raman intensities of the various TO and LO modes. Relative EO

values deduced from calculations are in fairly good agreement with the direct measurement of the EO and SHG coefficients. This corroborates the validity of the model used and the abilities of the approach to estimate the coefficients. Thus, the relative influence of doping on EO and SHG coefficients can be determined from Raman data, which just need a small crystal volume, whereas direct measurements require several large samples.

References

[1] Adachi M, Shiosaki T, Kobayashi H, Ohnishi O and Kawabata A 1985 *Ultrason. Symp.* 228
[2] Maeda M, Tachi H, Honda K and Suzuki I 1994 *Japan. J. Appl. Phys.* **33** 1965
[3] Matsuo T, Yagami T and Katsumata T 1993 *J. Appl. Phys.* **74-12** 7264
[4] Komatsu R, Sugawara T and Sassa K 1997 *Appl. Phys. Lett.* **70-26** 3492
[5] Krogh-Moe J 1962 *Acta Crystallogr.* **15** 190
[6] Zhigadlo N D 1995 *Phys. Status Solidi* a **152** 329
[7] Zaretskii V and Melzer R 1992 *Ferroelectrics* **125** 221
[8] Elbelrhiti Elalaoui A, Maillard A and Fontana M D 2003 *Ferroelectrics* **57–66** 296
[9] Paul G and Taylor W 1982 *J. Phys. C: Solid State Phys.* **15** 1753
[10] Furusawa S I, Tange S, Ishibashi Y and Miwa K 1990 *J. Phys. Soc. Japan* **59-5** 1825
[11] Adamiv V, Burak Y, Kityk I, Kasperczyk J, Smok R and Czerwinski M 1997 *Opt. Mater.* **8** 207
[12] Ilczyszyn M M 2000 *J. Mol. Struct.* **519** 257
[13] Johnston W D 1970 *Phys. Rev.* B **1–8** 3494
[14] Kaminov I P and Johnston W D 1967 *Phys. Rev.* **160–163** 519
[15] Wemple S H and Didomenico M 1972 Electrooptical and nonlinear optical properties of crystals *Applied Solid State Sciences* vol 3, ed R Wolfe (New York: Academic) p 264
[16] Fontana M D, Laabidi K and Carabatos-Nedelec C 1989 *Ferroelectrics* **94** 97
[17] Fontana M D, Laabidi K, Jannot B, Maglione M and Jullien P 1994 *Solid State Commun.* **92-10** 827
[18] Kwon T Y, Ju J J, Kim H K, Kim D J, Cha J W, Kim J N, Yum S I and Cha M 1997 *Mater. Lett.* **30** 293
[19] Bohaty P, Haussühl S and Liebertz J 1989 *Cryst. Res. Technol.* **24-11** 1159
[20] Burak Y, Dovgii Y and Kityk I 1990 *Zh. Prikl. Spektrosk.* **52-1** 126
[21] Lin Y, Xiong G, Lan G, Wang H and Xu L 1994 *J. Phys. Chem. Solids* **55-1** 113
[22] Jiang Y, Wang Y and Zeng L 1996 *J. Raman Spectrosc.* **27** 601
[23] Yufang W, Jianjun L, Shifen H and Guoxiang L 1999 *Spectrochim. Acta* A **55-13** 2565